RZ 3194 (# 93240) 01/03/00
Engineering & Technology 16 pages

Research Report

Achievable Bit Rates of DMT and FMT Systems in the Presence of Phase Noise and Multipath

N. Benvenuto[1], G. Cherubini[2] and L. Tomba[1]

[1]Dipartimento di Elettronica e Informatica
University of Padova
35131 Padova
Italy

[2]IBM Research
Zurich Research Laboratory
8803 Rüschlikon
Switzerland

Achievable Bit Rates of DMT and FMT Systems in the Presence of Phase Noise and Multipath*

N. Benvenuto[1], G. Cherubini[2] and L. Tomba[1]

[1]*Dipartimento di Elettronica e Informatica, University of Padova, 35131 Padova, Italy*

[2]*IBM Research, Zurich Research Laboratory, 8803 Rüschlikon Switzerland*

Abstract

Multicarrier systems based on orthogonal frequency division multiplexing (OFDM) are well suited for application in broadband radio access networks because of their intrinsic robustness for transmission over very dispersive multipath fading channels. In this paper we examine a modulation technique related to OFDM, called *filtered multitone* (FMT) modulation, which exhibits significantly lower spectral overlapping between adjacent subchannels than other OFDM schemes, such as *discrete multitone* (DMT). In particular, we present a comparison of the performance of FMT and DMT systems in the presence of phase noise introduced by the frequency down-conversion circuit, as well as multipath fading of the radio channel. As a measure of system performance we consider the *achievable bit rate*, which is evaluated by a general analytical procedure.

*This work has been supported in part by MURST (Roma, Italy) in the framework of the project "Variable rate mobile multimedia systems".

1 INTRODUCTION

Wireless local area networks (WLAN) and wireless asynchronous transfer mode (ATM) are emerging as solutions for wideband wireless access. In particular, WLANs allow computer networks to be established in dynamic environments. A first standard for WLANs where stations transmit information at high bit rates (23.5 Mbit/s) was HIPERLAN Type 1 [1], issued by the European Telecommunications Standards Institute (ETSI) RES-10 Group. A further development was HIPERLAN Type 2 [2], intended for local wireless access to ATM networks. Moreover, it provides short-range broadband wireless access to Internet Protocol (IP) networks and to the Universal Mobile Telecommunication System (UMTS). Another proposal in the area of broadband radio access networks (BRAN) is HIPERLINK [3], which would provide point-to-point interconnection at very high data rates, up to 155 Mbit/s, over distances up to 150 m.

The current proposal for HIPERLAN Type 2 physical layer (see ETSI Project BRAN #9) is based on DMT modulation [4], which can be regarded as a version of OFDM employing $\mathcal{M}$ orthogonal subcarriers for parallel transmission of blocks of $\mathcal{M}$ symbols over $\mathcal{M}$ subchannels. The peculiarity of DMT systems is that the modulation/demodulation processes are efficiently implemented by means of fast Fourier transformations. Moreover, equalization of dispersive radio channels is obtained by the simple mechanism of multiplying the signal at the output of each subchannel by one complex gain related to the channel frequency response. However, this simple scheme requires that redundancy be inserted in the modulated signal in the form of a prefix, the length of which is at least equal to that of the overall channel impulse response.

These considerations motivate the investigation of OFDM architectures with higher spectral efficiency. In this paper, we consider a filter-bank [5] modulation scheme related to OFDM, which is called *filtered multitone* (FMT) modulation [6, 7, 8], that exhibits significantly lower spectral overlapping between adjacent subchannels than DMT. In FMT systems, orthogonality between signals transmitted over different subchannels is obtained without the need for a cyclic prefix. Signal distortion is compensated by per-subchannel equalization, which is achieved, for example, by employing decision feedback equalizers (DFE). In general, some amount of excess bandwidth may be considered for transmission within a subchannel. Equalization may then be performed by fractionally spaced equalizers, which simplifies the synchronization circuits at the receiver [9].

In this paper, we focus on the performance comparison of DMT and FMT systems in the presence of multipath fading, and phase noise introduced by the frequency down-conversion circuit at the receiver. For a given channel, we consider the *achievable bit rate* as the measure of system performance [10], which is given by the sum of the bit rates each subchannel is eligible to deliver with a certain bit error rate. System performance is evaluated by an analytical procedure. With regard to other works on the same subject [11], here we also take into account the filtering operations both at the transmitter and the receiver side.

In our study the radio channel is approximated as being static, i.e., the Doppler spread is considered negligible within a few OFDM symbols corresponding to the transmission of one packet. However, because of the large extensions of the environments where the stations are intended to operate, the channel dispersion may be significant when compared to the modulation interval. For the channels considered here, it turns out that in terms of achievable bit rates, FMT systems are significantly more efficient than DMT for a number of subchannels limited to 128. This increase in efficiency is obtained at the expense of larger implementation complexity due to per-subchannel equalization. The loss in efficiency experienced by DMT systems becomes negligible for a large number of subchannels, e.g., more than 256.

The paper is organized as follows. In Section 2 we illustrate the filter-bank system model on which we rely for our analysis. In Section 3, features of the radio channel are discussed. In Section 4 we present a unified analysis for the general modulation scheme. The signal-to-distortion ratio is evaluated for each subchannel by taking into account the equalization achieved by appropriate filters. In Section 5 we compare the performance of DMT and FMT systems for different values of the parameters involved.

2 SYSTEM MODEL

Figure 1 illustrates the block diagram of the baseband equivalent of a filter-bank modulation scheme [5, 12]. In this system[1] the m-th, $0 \leqslant m < \mathcal{M}$, subchannel complex symbols data sequence, $d_m(i)$, $i \in \mathbb{Z}$, with symbol rate $1/T$, is upsampled by a factor of $\mathcal{K}$ (even) and filtered by a pulse shaping filter with impulse response $h_m(n)$. At the receiver side, dual transformations are implemented. We denote by $g_m(n)$ the impulse response of the m-th receive filter. In Fig. 1 $c(t)$ denotes the baseband equivalent channel impulse response, and A/D and D/A denote, respectively, the analog-to-digital and the digital-to-analog converters. In the A/D and D/A converter blocks, filtering operations are included that approximate ideal square-root raised cosine low-pass filtering with Nyquist frequency $\mathcal{K}/(2T)$. The overall discrete-time channel impulse response is denoted by $c_o(n)$. The general structure of Fig. 1 allows us to introduce the following multicarrier schemes.

A *DMT System*

DMT is the most popular and the conceptually simplest OFDM scheme. In this case $\mathcal{K} = \mathcal{M}$, $f_m = \frac{m}{T}$, $0 \leqslant m < \mathcal{M}$, and $h_m(n)$ is a rectangular pulse, namely

$$h_m(n) = \begin{cases} \frac{1}{T} & , \quad 0 \leqslant n < \mathcal{M} \\ 0 & , \quad \text{otherwise} \end{cases} . \tag{1}$$

Moreover, $g_m(n) = h_m^*(-n)$. Hence, all subchannels overlap in frequency. Perfect reconstruction of the transmitted sequences is possible, i.e., neither interchannel interference (ICI) nor intersymbol interference (ISI) is present on each subchannel, provided an ideal channel is considered.

To maintain orthogonality of signals over different subchannels, the transmitted frames in a DMT system are usually extended with a prefix of length $\mathcal{C}$. If $L_0 + 1$ is the support of $c_o(n)$ in number of samples and we choose $\mathcal{C} \geqslant L_0$, it is well known [4] that both ICI and ISI can be avoided. From an *analytical point of view*, a DMT system with a cyclic prefix can be obtained from the scheme in Fig. 1 by assuming $\mathcal{K} = \mathcal{M} + \mathcal{C}$, $f_m = 0$, $0 \leqslant m < \mathcal{M}$, and

$$h_m(n) = \begin{cases} \frac{1}{T}\, e^{j2\pi mn/\mathcal{M}} & , \quad -\mathcal{C} \leqslant n < \mathcal{M} \\ 0 & , \quad \text{otherwise} \end{cases} , \tag{2}$$

$$g_m(n) = \begin{cases} \frac{\mathcal{K}}{\mathcal{M}T}\, e^{j2\pi mn/\mathcal{M}} & , \quad -\mathcal{M} < n \leqslant 0 \\ 0 & , \quad \text{otherwise} \end{cases} . \tag{3}$$

For an efficient implementation of the DMT system, either with or without a prefix, carried out by an IDFT we refer to several papers (see [4, 10, 13] and references therein for more details). Here we mention that, in the DMT with a prefix, modulation of blocks of $\mathcal{M}$ input symbols is performed by the IDFT at the rate $\mathcal{M}/T \leqslant \mathcal{K}/T = (\mathcal{M} + \mathcal{C})/T$. In fact, after modulation, each block of $\mathcal{M}$ samples at the output of the IDFT is cyclically extended by copying the last $\mathcal{C}$ samples in front of the block. The sequence obtained is transmitted over the channel at the rate $\mathcal{K}/T$. At the receiver, blocks of samples of length $\mathcal{K}$ are taken. The first $\mathcal{C}$ samples are discarded and the last $\mathcal{M}$ samples of the block are demodulated by the DFT.

If $\mathcal{C} \geqslant L_0$, equalization of a DMT system is rather simple. In particular, with reference to the scheme of Fig. 2a and in the absence of noise, we have

$$\tilde{x}_m(i\mathcal{K}) = \alpha_m d_m(i) \tag{4}$$

[1] **Notation.** $\mathbb{E}[\cdot]$, $\Re[\cdot]$, $\Im[\cdot]$, j, $*$, $\mathbb{Z}, \mathbb{R}$, (I)DFT stand for expectation, real part, imaginary part, imaginary unit, complex conjugate, set of integer numbers, set of real numbers, (inverse) discrete Fourier transform, respectively. A signal and its corresponding Fourier transform are indicated by a lower and an upper-case letter, respectively.

where the coefficients $\{\alpha_m\}$, $m = 0, \ldots, \mathcal{M}-1$, are the samples of the $\mathcal{M}$-point DFT of the channel impulse response,[2]

$$\alpha_m = \sum_{k=0}^{L_0} \frac{T}{\mathcal{K}}\, c_o(k)\, e^{-j2\pi m(k-k_0)/\mathcal{M}} \ , \tag{5}$$

and k_0 is a suitably chosen delay. Once the coefficients $\{\alpha_m\}$ are known, e.g. by inserting known data (pilot symbols) at regular time intervals of length calculated on the basis of the maximum channel Doppler spread, equalization on each subchannel is obtained for example by dividing $\tilde{x}_m(i\mathcal{K})$ by α_m. If $\mathcal{C} \leqslant L_0$, interchannel interference arises and more complex equalization procedures, e.g., impulse response shortening [10, 14], must be introduced.

One drawback of DMT systems is the loss in spectral efficiency equivalent to a factor of $\zeta = \mathcal{M}/\mathcal{K}$. The ideal condition $\zeta \simeq 1$ is achieved only when the number of subchannels, $\mathcal{M}$, is much larger than the length of the channel impulse response, so that reduction in the data rate due to the cyclic extension may be considered negligible. Moreover, in DMT systems, to limit distortion $\mathcal{V}$ virtual subchannels,[3] i.e., subchannels with null input symbols, are usually inserted in the roll-off region of the D/A interpolation filter [4].

B *FMT System*

The above considerations motivate the investigation of FMT systems, which are obtained from the scheme in Fig. 1 by assuming that all subchannel filters $h_m(n)$ are equal to a given *prototype filter*, say $h_m(n) \equiv h(n)$, and equally spaced carrier frequencies, i.e., $f_m = \frac{m\mathcal{K}}{\mathcal{M}T}$. At the receiver, we choose $g_m(n) \equiv g(n) = h^*(-n)$. If $\mathcal{K} = \mathcal{M}$ we get a so-called *critically sampled* system [15], whereas if $\mathcal{K} > \mathcal{M}$ we get a *non-critically sampled* system [5, 6]. Here the filter $h(n)$ is a linear phase FIR filter appropriately designed to have an out-of-band energy lower than 40 dB with respect to the in-band energy such that, to a good approximation, we can write

$$H(f) = \begin{cases} \left| \frac{1+e^{-j2\pi f\mathcal{M}T/\mathcal{K}}}{1+\rho e^{-j2\pi f\mathcal{M}T/\mathcal{K}}} \right| & , \quad |f| < \frac{\mathcal{K}}{2\mathcal{M}T} \\ 0 & , \quad \text{otherwise} \end{cases} , \tag{6}$$

where $\rho = 0.9$. As the orthogonality conditions do not hold for transmission within a subchannel, it is necessary to equalize the signal further to eliminate ISI introduced by both the filters and the channel. On the other hand, residual ICI can be considered negligible even for moderate lengths of the prototype filter. In order to simplify the receiver, we use an equalizer that consists of two parts (see Fig. 2b):

1. A complex gain that compensates for the gain/rotation introduced by the dispersive channel, as in DMT systems. This coefficient can be determined by channel identification and can be made adaptive. This procedure assumes that the channel coherence bandwidth is much greater than $1/T$ so that each subchannel approximately behaves like a flat-fading one.

2. A fixed DFE that compensates for the ISI. When $\mathcal{K} > \mathcal{M}$ a $T/2$ fractionally spaced DFE can be used [6] and the system is labelled FMT-FS (scheme shown in Fig. 2b).

By using standard procedures [9], this equalizer is designed by taking into account the impulse responses of the prototype filter $h(n)$, D/A and A/D filter $g_I(t)$, and an expected signal-to-noise ratio (SNR) for transmission in the presence of the additive white Gaussian noise (AWGN) $\eta(n)$ with power spectral density (PSD) is N_0. The SNR is defined as

$$\mathrm{SNR} = \frac{\mathbb{E}\left[|r(n)|^2\right]}{N_0\mathcal{K}/T} \ . \tag{7}$$

[2] In this paper the discrete-time Fourier transform of the sequence $x(n)$ with samples spaced of T is defined as $X(f) = \sum_{n=-\infty}^{\infty} T x(n) e^{-j2\pi f nT}$.

[3] Usually $\mathcal{V}$ is assumed to be even because the virtual carriers are evenly divided at the edges of the D/A and A/D filter frequency responses.

3 CHANNEL MODEL

The radio channel is represented by a baseband impulse response, $c(t)$, given by

$$c(t) = \sum_{p=0}^{\mathcal{P}-1} c_p \, \delta(t - \tau_p) \quad , \qquad t \in \mathbb{R} \quad , \tag{8}$$

where $\mathcal{P}$ is the number of paths, c_p is the complex gain of the p-th path, $\delta(\cdot)$ is the Dirac pulse and τ_p is the delay of the p-th path. Here $\{c_p\}$ are assumed to be zero-mean, independent complex Gaussian random variables with an exponentially power delay profile [16]. The actual number of paths, $\mathcal{P}$, depends on the root-mean-square (rms) delay spread, σ_c, of the channel and may be of the order of some hundred of ns if large areas are considered [16]. Here, the rms delay spread normalized to the system bandwidth, $\sigma_\tau = \sigma_c \mathcal{K}/T$, will be considered. The channel impulse response, in the form given by (8), represents a static channel, as we assume for the duration of one data packet. However, to get meaningful performance measures, several realizations of the channel impulse response will be generated.

Possible non-ideal behaviors of the synchronization circuits may introduce further performance degradation of the system. In particular, phase noise plays a fundamental role in OFDM signals transmitted in the frequency region of 5 GHz (HIPERLAN) and 17 GHz (HIPERLINK) and possibly 40 GHz [11, 17]. In this work, we assume that the frequency down-conversion circuit consists both of a voltage controlled oscillator and a digital phase-locked loop [18]. Hence, on the basis of the results reported in [19, 20], the residual phase noise $\vartheta(t)$ can be modeled by a stationary zero-mean Gaussian process independent of the received microwave signal. The zero-mean assumption for $\vartheta(\cdot)$ implies that a possible phase offset is exactly compensated at the receiver. The PSD of $\vartheta(\cdot)$ is given by[4]

$$\overline{\mathcal{S}}_\vartheta(f) = 10^{-c_\vartheta} + \begin{cases} 10^{-a_\vartheta} & , \quad |f| \leqslant f'_\vartheta \\ 10^{-(|f|-f'_\vartheta) b_\vartheta / (f''_\vartheta - f'_\vartheta) - a_\vartheta} & , \quad |f| > f'_\vartheta \end{cases} \quad . \tag{9}$$

Typical values for the parameters may be $a_\vartheta = 7.5$, $b_\vartheta = 4$, $c_\vartheta = 10.5$, $f'_\vartheta = 1$ kHz and $f''_\vartheta = 10$ kHz [19, 20]. The value of c_ϑ determines the noise floor, which has been assumed at -105 dB. Because of the values of f'_ϑ and f''_ϑ, a reduction of the PSD of 40 dB/decade is assumed. However, various values of the above parameters will be considered, as they are dependent on the tuner technology used. In the baseband model of Fig. 1 the phase noise contribution is taken into account by the product term $e^{j\vartheta(n)}$, which introduces a phase rotation of $\vartheta(n)$. By assuming the standard deviation of $\vartheta(n)$, $\sigma_\vartheta \ll 1$, we can write to a good approximation

$$e^{j\vartheta(n)} \simeq 1 + j\vartheta(n) \; . \tag{10}$$

4 DISTORTION EVALUATION

In this section we evaluate, by using a general analytical approach, the error on each subchannel of the filter-bank modulation scheme of Fig. 1, which is given by

$$\xi_m(i) \equiv s_m(i) - d_m(i - \Delta) \quad , \qquad 0 \leqslant m < \mathcal{M} \; , \tag{11}$$

where Δ is the delay introduced by the system. In general $\xi_m(i)$ is due to modulation filters, multipath, phase noise and channel noise. Here we assume that the input data sequences are complex-valued, zero-mean, independent and wide-sense stationary random processes. This means that

$$\mathbb{E}\,[d_m(i)] = 0 \quad \text{and} \quad \overline{\mathcal{S}}_{d_m d_n}(f) = \overline{\mathcal{S}}_{d_m}(f) \delta_{mn} \; , \tag{12}$$

[4] Some processes involved in the scheme in Fig. 1 turn out to be cyclostationary and their correlation function depends both on the reference instant and the shift; consequently, their PSD is the bidimensional Fourier transform of the correlation function. The spectral density of a stationary signal, instead, is a function of one variable and will be denoted by $\overline{S}(f)$.

where δ_{mn} is the Kronecker delta. In this work, based on the central limit theorem [21], we also assume that the error (11) is a Gaussian process. In particular, the real and the imaginary parts of $\xi_m(i)$ are zero-mean, equal power, uncorrelated Gaussian random variables [22]. The power of (11) is given by

$$M_{\xi_m} = \mathbb{E}\left[|s_m(i) - d_m(i-\Delta)|^2\right] = \mathbb{E}\left[|s_m(i)|^2\right] - 2\,\Re\{\mathbb{E}[s_m(i)d_m^*(i-\Delta)]\} + \mathbb{E}\left[|d_m(i-\Delta)|^2\right] \ . \quad (13)$$

As $s_m(i) = v_m(i) + w_m(i)$ (see Fig. 2b), the first two terms in (13) can be written as

$$\mathbb{E}\left[|s_m(i)|^2\right] = \mathbb{E}\left[|v_m(i)|^2\right] + \mathbb{E}\left[|w_m(i)|^2\right] + 2\,\Re\{\mathbb{E}[v_m(i)w_m^*(i)]\} \quad (14)$$

and

$$\mathbb{E}[s_m(i)d_m^*(i-\Delta)] = \mathbb{E}[v_m(i)d_m^*(i-\Delta)] + \mathbb{E}[w_m(i)d_m^*(i-\Delta)] \ . \quad (15)$$

For the computation of the expectations of the above signals we evaluate the corresponding average PSD and then we calculate their integral over $[0, 1/T)$ [9]. For example, (14) becomes

$$M_{s_m} = \int_0^{1/T} \left[\overline{\mathcal{S}}_{v_m}(f) + \overline{\mathcal{S}}_{w_m}(f) + 2\,\Re\left\{\overline{\mathcal{S}}_{v_m w_m}(f)\right\}\right] df \ , \quad (16)$$

whereas (13) can be written as

$$M_{\xi_m} = \int_0^{1/T} \left[\overline{\mathcal{S}}_{v_m}(f) + \overline{\mathcal{S}}_{w_m}(f) + \overline{\mathcal{S}}_{d_m^\Delta}(f) + 2\,\Re\left\{\overline{\mathcal{S}}_{v_m w_m}(f) - \overline{\mathcal{S}}_{v_m d_m^\Delta}(f) - \overline{\mathcal{S}}_{w_m d_m^\Delta}(f)\right\}\right] df \ , \quad (17)$$

where d_m^Δ denotes the sequence $d_m(i-\Delta)$. By using a general procedure, outlined in Appendix A, expression of each PSD in (16) and (17) is reported in Appendix B. For a given channel, the ratio

$$\mathrm{SNDR}_m = \frac{M_{s_m}}{M_{\xi_m}} \quad (18)$$

represents the signal-to-error (noise plus distortion) power ratio on the mth subcarrier.

5 NUMERICAL RESULTS

Here we report the results of a performance comparison of DMT and FMT systems in the presence of multipath and phase noise. The results are obtained under the following assumptions:

- the available transmission bandwidth is the same for both DMT and FMT, equal to $\mathcal{K}/T = 25$ MHz;
- ideal estimation of subchannel gains is performed, i.e., the channel impulse response is *known*;
- ideal compensation of a possible phase offset is carried out at regular time intervals, thus the phase noise has zero mean.

The phase noise spectral density has been chosen with the parameter values of Section 3. The D/A and A/D low pass filters belong to the square-root Nyquist class with the following characteristics: *(i)* unitary gain, *(ii)* Nyquist frequency $= \mathcal{K}/2T$, *(iii)* roll-off factor $= 0.07$ and *(iv)* attenuation $= -50$ dB. For DMT the cyclic prefix length, $\mathcal{C}$, has been set at $\lfloor 5\sigma_\tau \rfloor$; moreover, owing to the slowly decaying characteristics of the prototype filter frequency response, the number $\mathcal{V}$ of virtual carriers was selected equal to $1/16$ of the number of subcarriers $\mathcal{M}$, i.e., 4, 8, and 16 for $\mathcal{M}$ equal to 64, 128, and 256, respectively. Higher values of $\mathcal{V}$ yield a greater signal-to-distortion ratio (SDR) at the expense of lower spectral efficiency. However, the gain in SDR may be not significant compared to the SNR values of 20–25 dB considered here.

For FMT systems, only two virtual carriers have been assumed, independent of the number $\mathcal{M}$ of subchannels. Per-subchannel equalization is achieved by T-spaced or fractionally $T/2$-spaced DFE, as described in Section 2. The number of coefficients of the linear feed-forward filters is chosen equal to 16 for both FMT and FMT-FS. The lengths of the feedback filters are 15 and 8, respectively, for FMT and FMT-FS.

It is interesting to report values of the signal-to-noise plus distortion ratio SNDR_m at the decision point of the m-th subchannel. In particular, in Table 1 we report the normalized degradation, $\mathcal{D}_m$, due to various system and channel impairments,

$$\mathcal{D}_m = \frac{\mathrm{SNR}}{\mathrm{SNRD}_m} \ , \tag{19}$$

for $m = \mathcal{M}/2$, the central subchannel, and an ideal AWGN channel with SNR of 25 dB. We see that the best performance is achieved by DMT and that FMT and FMT-FS achieve similar performances. We remark that this behavior depends on the parameters chosen for the prototype and DFE filters. For example, an FMT-FS system employing an ideal prototype filter with square-root raised cosine characteristic would also exhibit zero normalized degradation. We also remark that the impact of phase noise is more apparent on FMT than on DMT because of the longer impulse response of the prototype filter.

However, for a fair comparison of different systems, as a performance measure we consider the achievable bit rate. We introduce the modified SNDR_m, in dB, as [9, 10]

$$(\overline{\mathrm{SNDR}}_m)_{\mathrm{dB}} = (\mathrm{SNDR}_m)_{\mathrm{dB}} - 12.8 \ , \tag{20}$$

where the value of 12.8 dB has been calculated assuming a bit error rate of 10^{-7} and a coding gain of 3 dB. Then, the achievable bit rate β_m on the m-th subchannel for given channel characteristics is expressed as

$$\beta_m = \frac{1}{T} \ \log_2(\overline{\mathrm{SNDR}}_m + 1) \quad , \qquad [\mathrm{bit/s}] \ , \tag{21}$$

where $\frac{1}{T} = \frac{25}{\mathcal{K}}[\mathrm{Mbaud}]$ for FMT and $\frac{1}{T} = \frac{25}{\mathcal{M}+\mathcal{C}}[\mathrm{Mbaud}]$ for DMT. In turn, the achievable bit rate β is obtained by summing up the values given by (21) over the active subchannels allocated for transmission, i.e.

$$\beta = \sum_{m=\mathcal{V}/2}^{\mathcal{M}-1-\mathcal{V}/2} \beta_m \quad , \qquad [\mathrm{bit/s}] \ . \tag{22}$$

For comparison purposes we consider the complementary cumulative distribution function of β evaluated over 500 realizations of the multipath fading channel. In our numerical results we have assumed channels with three normalized rms delay spread, namely $\sigma_\tau = 1$, 2 and 4.

For three values of the phase noise ($a_\vartheta = \infty$ corresponds to no phase noise) and three values of the multipath rms delay spread, in Figure 3 and 4 we show the achievable bit rate β for a DMT system with $\mathcal{M} = 64$ and $\mathcal{M} = 128$, respectively. It is apparent that β improves as $\mathcal{M}$ increases. Moreover, the phase noise may affect β especially for higher values of $\mathcal{M}$ and when the channel has a low dispersion.

Similar curves are reported in Figure 5 and 6 for a FMT system with $\mathcal{K} = \mathcal{M} = 64$ and $\mathcal{K} = \mathcal{M} = 128$, respectively. Also for FMT, for large values of $\mathcal{M}$, performance is affected by the presence of phase noise. In any case, performance of FMT is significantly better than that of DMT.

Figure 7 shows a comparison between FMT and FMT-FS for different values of $\mathcal{M}$ and $\mathcal{K}$ in the absence of phase noise. From the results it appears that it is not desirable to choose $\mathcal{M}$ much lower than $\mathcal{K}$. Slightly better behavior of FMT-FS with respect to FMT is seen for higher values of σ_τ. Similar behaviour is seen also in the presence of phase noise (results not shown). Finally, Fig. 8 shows the same comparison of Fig. 7 when $\mathcal{K} = 128$ instead of $\mathcal{K} = 64$. As the DFE filters for FMT-FS have a shorter time span, FMT-FS yields worse performance than FMT.

In conclusion all results show a higher spectral efficiency of FMT and FMT-FS with respect to DMT. Indeed, for a given bandwidth, there is no need for a cyclic prefix nor for many virtual carriers in FMT due to the negligible spectral overlapping between adjacent subchannels. This allows for reliable transmission over subchannels where no transmission is possible for a DMT system, unless a substantially higher D/A e A/D filter complexity is afforded. Moreover, the slightly better behavior of DMT in the presence of phase noise is compensated and exceeded by the better spectral efficiency of FMT. However, we remark that the better performance of FMT is achieved at the expense of additional computational complexity required by per-subchannel equalization.

In summary, the robustness and efficiency of FMT suggest its use for HIPERLAN and HIPERLINK transceivers.

6 CONCLUSION

In this paper we have considered two transmission schemes, namely DMT and FMT, which are suitable for application to HIPERLAN Type 2 and HIPERLINK transceivers. The performance of the two systems has been investigated assuming very dispersive Rayleigh fading channels, and taking into account the presence of phase noise introduced by the frequency tuner at the receiver side. The results, expressed in terms of achievable bit rates, indicate that FMT exhibits a significantly higher efficiency than DMT, also in the presence of non negligible phase noise. For the application considered, satisfactory per-subchannel equalization in FMT systems is achieved by a fixed T-spaced or fractionally-spaced DFE and a variable complex gain.

APPENDIX A

General Procedure

We briefly recall the basic steps of the spectral analysis method, which will be used in Appendix B. We assume that $x(\cdot)$ is a (in general) non-stationary process and $y(\cdot)$ is a random process obtained by a linear transformation of $x(\cdot)$. We want to evaluate the PSD of $y(\cdot)$. For this purpose, we first determine the relationship between their Fourier transforms, $Y(\cdot)$ and $X(\cdot)$, respectively. Then, we evaluate the product $Y(f)Y^*(f-\lambda)$ and formally replace $Y(f)Y^*(f-\lambda)$ by $\mathcal{S}_y(\lambda, f)$ and $X(f')X^*(f'-\lambda')$ by $\mathcal{S}_x(\lambda', f')$ [21]. To motivate this approach we remark that, when dealing with cyclostationary processes, it is not always possible to carry out spectral analysis by using the relationships that hold between the average PSDs.

APPENDIX B

Spectral Density Evaluation

By using the method outlined in Appendix A, five spectral evaluations are reported.
1. EVALUATION OF $\overline{\mathcal{S}}_{v_m}(f)$. This evaluation is split into three steps: *(i)* PSD of $r(n)$, *(ii)* PSD of $\tilde{r}(n)$ and *(iii)* PSD of $v_m(i)$ (signals $\tilde{r}(\cdot)$ and $v_m(i)$ are defined in Fig. 1).
(i) $\mathcal{S}_r(\lambda, f)$*:* The Fourier transform of $r(n)$ is

$$R(f) = C_o(f) \sum_{m=\mathcal{V}/2}^{\mathcal{M}-1-\mathcal{V}/2} D_m(f-f_m)H_m(f-f_m)\ . \tag{B1}$$

Hence

$$\begin{aligned} R(f)R^*(f-\lambda) = C_o(f)C_o^*(f-\lambda) &\sum_{m_1=\mathcal{V}/2}^{\mathcal{M}-1-\mathcal{V}/2} D_{m_1}(f-f_{m_1})H_{m_1}(f-f_{m_1}) \\ \times &\sum_{m_2=\mathcal{V}/2}^{\mathcal{M}-1-\mathcal{V}/2} D_{m_2}^*(f-\lambda-f_{m_2})H_{m_2}^*(f-\lambda-f_{m_2})\ , \end{aligned} \tag{B2}$$

and

$$\begin{aligned}\mathcal{S}_r(\lambda,f) = & C_o(f)C_o^*(f-\lambda)\sum_{m_1=\mathcal{V}/2}^{\mathcal{M}-1-\mathcal{V}/2} H_{m_1}(f-f_{m_1}) \\ & \times \sum_{m_2=\mathcal{V}/2}^{\mathcal{M}-1-\mathcal{V}/2} H_{m_2}^*(f-\lambda-f_{m_2})\mathcal{S}_{d_{m_1}d_{m_2}}(\lambda+f_{m_2}-f_{m_1},f-f_{m_1})\,.\end{aligned} \tag{B3}$$

From the assumption on the statistics of the input data sequences we get

$$\mathcal{S}_{d_{m_1}d_{m_2}}(\lambda,f) = \mathcal{S}_{d_{m_1}}(\lambda,f)\,\delta_{m_1m_2} = \overline{\mathcal{S}}_{d_{m_1}}(f)\sum_{p=-\infty}^{\infty}\delta\left(\lambda+\frac{p}{T}\right)\delta_{m_1m_2}\,, \tag{B4}$$

where $\overline{\mathcal{S}}_{d_{m_1}}(f)$ is the average PSD of $d_{m_1}(i)$ and $\delta(t)$ is the Dirac delta. In conclusion, by introducing (B4) in (B3), we obtain

$$\mathcal{S}_r(\lambda,f) = C_o(f)C_o^*(f-\lambda)\sum_{m=\mathcal{V}/2}^{\mathcal{M}-1-\mathcal{V}/2} H_m(f-f_m)H_m^*(f-\lambda-f_m)\overline{\mathcal{S}}_{d_m}(f-f_m)\sum_{p=-\infty}^{\infty}\delta\left(\lambda+\frac{p}{T}\right) \tag{B5}$$

(ii) $\mathcal{S}_{\tilde{r}}(\lambda,f)$*:* By using (1) approximation (10), (2) the statistical independence among $r(n)$, $\vartheta(n)$ and $\eta(n)$, and (3) $\mathbb{E}[\vartheta(n)] = \mathbb{E}[\eta(n)] = 0$, we get

$$\mathcal{S}_{\tilde{r}}(\lambda,f) = \mathcal{S}_r(\lambda,f) + [\mathcal{S}_r(\lambda,f')\odot\overline{\mathcal{S}}_\vartheta(f')](\lambda,f) + \mathcal{S}_\eta(\lambda,f)\,, \tag{B6}$$

where $\odot$ denotes *cyclic convolution* [23].
(iii) $\mathcal{S}_{v_m}(\lambda,f)$*:* We obtain

$$V_m(f) = \alpha_m\sum_{h=0}^{1} Q_{\text{FF}}\left(f+\frac{h}{T}\right)\sum_{k=0}^{\mathcal{K}/2-1} G_m\left(f+\frac{h+2k}{T}\right)\tilde{R}\left(f+f_m+\frac{h+2k}{T}\right)\,, \tag{B7}$$

and

$$\begin{aligned}V_m(f)V_m^*(f-\lambda) = & |\alpha_m|^2\sum_{h_1=0}^{1} Q_{\text{FF}}\left(f+\frac{h_1}{T}\right)\sum_{k_1=0}^{\mathcal{K}/2-1} G_m\left(f+\frac{h_1+2k_1}{T}\right)\tilde{R}\left(f+f_m+\frac{h_1+2k_1}{T}\right) \\ & \times\sum_{h_2=0}^{1} Q_{\text{FF}}^*\left(f-\lambda+\frac{h_2}{T}\right)\sum_{k_2=0}^{\mathcal{K}/2-1} G_m^*\left(f-\lambda+\frac{h_2+2k_2}{T}\right)\tilde{R}^*\left(f-\lambda+f_m+\frac{h_2+2k_2}{T}\right)\,,\end{aligned} \tag{B8}$$

which yields

$$\begin{aligned}\mathcal{S}_{v_m}(\lambda,f) = & |\alpha_m|^2\sum_{h_1=0}^{1} Q_{\text{FF}}\left(f+\frac{h_1}{T}\right)\sum_{k_1=0}^{\mathcal{K}/2-1} G_m\left(f+\frac{h_1+2k_1}{T}\right)\sum_{h_2=0}^{1} Q_{\text{FF}}^*\left(f-\lambda+\frac{h_2}{T}\right) \\ & \times\sum_{k_2=0}^{\mathcal{K}/2-1} G_m^*\left(f-\lambda+\frac{h_2+2k_2}{T}\right)\mathcal{S}_{\tilde{r}}\left(\lambda-\frac{h_2-h_1}{T}-\frac{2k_2-2k_1}{T},f+f_m+\frac{h_1+2k_1}{T}\right)\,.\end{aligned} \tag{B9}$$

As $\mathcal{S}_{\tilde{r}}(\lambda,f)$ is composed of three additive contributions [due, respectively, to $r(\cdot)$, $\eta(\cdot)$ and $\vartheta(\cdot)$], we get, respectively

$$\mathcal{S}_{v_m}(\lambda,f) = \mathcal{S}_{v_m}^a(\lambda,f) + \mathcal{S}_{v_m}^b(\lambda,f) + \mathcal{S}_{v_m}^c(\lambda,f)\,. \tag{B10}$$

Now we start with the evaluation of $\mathcal{S}^{b}_{v_m}(\lambda, f)$. By using (B5), after some algebraic manipulations we obtain

$$\mathcal{S}^{b}_{v_m}(\lambda, f) = |\alpha_m|^2 \int_0^{\mathcal{K}/T} \sum_{n=\mathcal{V}/2}^{\mathcal{M}-1-\mathcal{V}/2} \left\{ \overline{\mathcal{S}}_{d_n}(f'-f_n)\mathcal{S}_{\vartheta}(f+f_m-f') \sum_{h_1=0}^{1} Q_{\text{FF}}\left(f+\frac{h_1}{T}\right) \right.$$
$$\times \sum_{k_1=0}^{\mathcal{K}/2-1} G_m\left(f+\frac{h_1+2k_1}{T}\right) C_o\left(f'+\frac{h_1+2k_1}{T}\right) H_n\left(f'-f_n+\frac{h_1+2k_1}{T}\right)$$
$$\times \sum_{h_2=0}^{1} Q^*_{\text{FF}}\left(f-\lambda+\frac{h_2}{T}\right) \sum_{k_2=0}^{\mathcal{K}/2-1} G^*_m\left(f-\lambda+\frac{h_2+2k_2}{T}\right) C^*_o\left(f'-\lambda+\frac{h_2+2k_2}{T}\right)$$
$$\left. \times H^*_n\left(f'-f_n-\lambda+\frac{h_2+2k_2}{T}\right) \right\} df' \sum_{p=-\infty}^{\infty} \delta\left(\lambda+\frac{p}{T}\right) . \tag{B11}$$

Moreover, by taking into account the periodicity of the functions in (B11), we further obtain

$$\mathcal{S}^{b}_{v_m}(\lambda, f) = \overline{\mathcal{S}}^{b}_{v_m}(f) \sum_{p=-\infty}^{\infty} \delta\left(\lambda+\frac{p}{T}\right) , \tag{B12}$$

where

$$\overline{\mathcal{S}}^{b}_{v_m}(f) = |\alpha_m|^2 \int_0^{\mathcal{K}/T} \sum_{n=\mathcal{V}/2}^{\mathcal{M}-1-\mathcal{V}/2} \left\{ \overline{\mathcal{S}}_{d_n}(f'-f_n)\overline{\mathcal{S}}_{\vartheta}(f+f_m-f') \right.$$
$$\left. \times \left| \sum_{h=0}^{1} Q_{\text{FF}}\left(f+\frac{h}{T}\right) \sum_{k=0}^{\mathcal{K}/2-1} G_m\left(f+\frac{h+2k}{T}\right) C_o\left(f'+\frac{h+2k}{T}\right) H_n\left(f'-f_n+\frac{h+2k}{T}\right) \right|^2 \right\} df' . \tag{B13}$$

It is apparent that (B13) yields the PSD $\mathcal{S}^{a}_{v_m}(\lambda, f)$ by letting $\overline{\mathcal{S}}_{\vartheta}(f) = \sum_{p=-\infty}^{\infty} \delta(f + p\mathcal{K}/T)$. The result is

$$\mathcal{S}^{a}_{v_m}(\lambda, f) = \overline{\mathcal{S}}^{a}_{v_m}(f) \sum_{p=-\infty}^{\infty} \delta\left(\lambda+\frac{p}{T}\right) , \tag{B14}$$

where

$$\overline{\mathcal{S}}^{a}_{v_m}(f) = |\alpha_m|^2 \sum_{n=\mathcal{V}/2}^{\mathcal{M}-1-\mathcal{V}/2} \overline{\mathcal{S}}_{d_n}\left(f+f_m-f_n\right)$$
$$\times \left| \sum_{h=0}^{1} Q_{\text{FF}}\left(f+\frac{h}{T}\right) \sum_{k=0}^{\mathcal{K}/2-1} G_m\left(f+\frac{h+2k}{T}\right) C_o\left(f+f_m+\frac{h+2k}{T}\right) H_n\left(f+f_m-f_n+\frac{h+2k}{T}\right) \right|^2 . \tag{B15}$$

For the evaluation of $\mathcal{S}^{c}_{v_m}(\lambda, f)$ we introduce the PSD of noise η, $\overline{\mathcal{S}}_{\eta}(f) = N_0$, in (B9) to obtain

$$\mathcal{S}^{c}_{v_m}(\lambda, f) = \overline{\mathcal{S}}^{c}_{v_m}(f) \sum_{p=-\infty}^{\infty} \delta\left(\lambda+\frac{p}{T}\right) , \tag{B16}$$

where

$$\overline{\mathcal{S}}^{c}_{v_m}(f) = N_0|\alpha_m|^2 \left| \sum_{h=0}^{1} Q_{\text{FF}}\left(f+\frac{h}{T}\right) \sum_{k=0}^{\mathcal{K}/2-1} G_m\left(f+\frac{h+2k}{T}\right) \right|^2 . \tag{B17}$$

2. EVALUATION OF $\overline{\mathcal{S}}_{w_m}(f)$. Sequence $w_m(i)$ is obtained from $d_m(i)$ by filtering operations; hence it is immediate to write [21]

$$\overline{\mathcal{S}}_{w_m}(f) = |Q_{\rm FB}(f)|^2\, \overline{\mathcal{S}}_{d_m}(f)\ . \tag{B18}$$

3. EVALUATION OF $\overline{\mathcal{S}}_{v_m w_m}(f)$. By applying the general procedure, we get

$$\begin{aligned} V_m(f)W_m^*(f-\lambda) = \alpha_m \sum_{h=0}^{1} Q_{\rm FF}\left(f+\frac{h}{T}\right) \sum_{k=0}^{\mathcal{K}/2-1} G_m\left(f+\frac{h+2k}{T}\right) \tilde{R}\left(f+f_m+\frac{h+2k}{T}\right) \\ \times Q_{\rm FB}^*(f-\lambda) D_m^*(f-\lambda) e^{j2\pi(f-\lambda)\Delta T} \end{aligned} \tag{B19}$$

which yields

$$\begin{aligned} \mathcal{S}_{v_m w_m}(\lambda,f) = \alpha_m \sum_{h=0}^{1} Q_{\rm FF}\left(f+\frac{h}{T}\right) \sum_{k=0}^{\mathcal{K}/2-1} G_m\left(f+\frac{h+2k}{T}\right) \\ \times Q_{\rm FB}^*(f-\lambda)\, e^{j2\pi(f-\lambda)\Delta T} \mathcal{S}_{\tilde{r}d_m}\left(\lambda+f_m+\frac{h+2k}{T}, f+f_m+\frac{h+2k}{T}\right)\ . \end{aligned} \tag{B20}$$

Now we observe that the correlation between $\tilde{r}(\cdot)$ and $d_m(\cdot)$ is

$$\mathbb{E}\left[\tilde{r}(t+\tau)d_m^*(t)\right] = \mathbb{E}\left[\left[r(t+\tau)+\eta(t+\tau)\right]\left[1+j\vartheta(t+\tau)\right]d_m^*(t)\right] = \mathbb{E}\left[r(t+\tau)d_m^*(t)\right]\ , \tag{B21}$$

so that in (B20) we may replace $\mathcal{S}_{\tilde{r}d_m}(\lambda,f)$ with $\mathcal{S}_{rd_m}(\lambda,f)$, whose expression is

$$\mathcal{S}_{rd_m}(\lambda,f) = C_o(f)H_m(f-f_m)\overline{\mathcal{S}}_{d_m}(f-f_m) \sum_{p=-\infty}^{\infty} \delta\left(\lambda-f_m+\frac{p}{T}\right)\ . \tag{B22}$$

The result is

$$\mathcal{S}_{v_m w_m}(\lambda,f) = \overline{\mathcal{S}}_{v_m w_m}(f) \sum_{p=-\infty}^{\infty} \delta\left(\lambda+\frac{p}{T}\right)\ , \tag{B23}$$

where

$$\begin{aligned} \overline{\mathcal{S}}_{v_m w_m}(f) = \alpha_m\, \overline{\mathcal{S}}_{d_m}(f)\, Q_{\rm FB}^*(f)\, e^{j2\pi f\Delta T} \\ \times \sum_{h=0}^{1} Q_{\rm FF}\left(f+\frac{h}{T}\right) \sum_{k=0}^{\mathcal{K}/2-1} G_m\left(f+\frac{h+2k}{T}\right) C_o\left(f+f_m+\frac{h+2k}{T}\right) H_m\left(f+\frac{h+2k}{T}\right)\ . \end{aligned} \tag{B24}$$

4. EVALUATION OF $\overline{\mathcal{S}}_{v_m d_m^\Delta}(f)$. It is apparent that this proof can be obtained as a particular case of the previous one. The result is

$$\mathcal{S}_{v_m d_m^\Delta}(\lambda,f) = \overline{\mathcal{S}}_{v_m d_m^\Delta}(f) \sum_{p=-\infty}^{\infty} \delta\left(\lambda+\frac{p}{T}\right)\ , \tag{B25}$$

where

$$\overline{\mathcal{S}}_{v_m d_m^\Delta}(f) = \overline{\mathcal{S}}_{v_m w_m}(f)/Q_{\rm FB}^*(f)\ . \tag{B26}$$

5. EVALUATION OF $\overline{\mathcal{S}}_{w_m d_m^\Delta}(f)$. As $w_m(i)$ is obtained from $d_m^\Delta(i)$ by filtering operations, we get

$$\overline{\mathcal{S}}_{w_m d_m^\Delta}(f) = Q_{\rm FB}(f)\, \overline{\mathcal{S}}_{d_m}(f)\ . \tag{B27}$$

REMARKS ON NUMERICAL COMPUTATION. The above formulas seem to require an extremely high computational complexity. Hence, it is worthwhile to say a few words about how to evaluate them in a

reasonable computing time. This issue is relevant because each value of SNDR_m must be evaluated for several realizations of the radio channel (typically 500 or more) in order to get fair average performance for a dynamic environment. The method adopted is very simple. First, we observe that the PSDs involved in (16) and (17) are very smooth (thanks to the fact the input sequences are assumed white) and a limited number of abscissas is required to evaluate the integrals. A precision of approximately 0.1 dB is obtained experimentally by using just 15 points in the numerical integration procedure. Hence, the various Fourier transforms need to be evaluated only on a limited set of frequencies. In particular these functions are evaluated only once, and stored in memory. In this way, computing time is reduced significantly.

References

[1] "Radio Equipment and Systems (RES): High PErformance Radio Local Area Network (HIPERLAN), Type 1 functional specification," *European Telecommunications Standards Institute* (ETSI), DRAFT PE6 prETS 300 652, France, Dec. 1995.

[2] "BRAN; HIgh PErformance Radio Local Area Network (HIPERLAN), Type 2; Requirements and architectures for wireless broadband access," *European Telecommunications Standards Institute* (ETSI), TR 101 031 V. 2.2.1, France, Jan. 1999.

[3] R. Prasad, H. Teunissen, "A state-of-the-art of HIPERLAN/2," *IEEE VTC '99 Fall*, pp. 2661-2666, Amsterdam, Sep. 1999.

[4] J.A.C. Bingham, "Multicarrier modulation for data transmission: an idea whose time has come," *IEEE Commun. Magazine*, vol. 28, no. 5, pp. 5–14, May 1990.

[5] R.E. Crochiere, L.R. Rabiner, *Multirate Digital Signal Processing.* Prentice-Hall, Inc., Englewood Cliffs, NJ, 1983.

[6] G. Cherubini, E. Eleftheriou, and S. Oelcer, "Advanced Multicarrier Modulation Techniques for xDSL," IEEE Circuits and Systems and Communications Societies Workshop on *High-Speed Data over Local Loops and Cables*, Princeton University, Princeton, New Jersey, July 26-28, 1999.

[7] G. Cherubini, E. Eleftheriou, and S. Oelcer, "Filtered Multitone Modulation for VDSL," to be presented at *GLOBECOM'99, IEEE Global Telecommunications Conference*, Rio de Janeiro, Brazil, Dec. 5-9, 1999.

[8] G. Cherubini, "A hybrid TDMA/CDMA system based on filtered multitone modulation for uplink transmission in HFC networks," submitted to *IEEE Trans. on Commun.*, Jan. 1999.

[9] J.G. Proakis, *Digital Communications*. 3$^{\mathrm{rd}}$ ed., New York, McGraw-Hill, 1995.

[10] J.M. Cioffi, "Asymmetrical Digital Subscriber Lines," in *The Communications Handbook*, J.D. Gibson (Ed.), CRC Press Inc., pp. 450–479, 1997.

[11] H. Steendam, M. Moeneclaey, H. Sari, "The effect of carrier phase jitter on the performance of orthogonal frequency-division multiple-access systems," *IEEE Trans. Commun.*, vol. 46, no. 4, pp. 456–459, Apr. 1998.

[12] P.P. Vaidyanathan, *Multirate Systems and Filter Banks.* Prentice Hall, Inc., Englewood Cliffs, NJ, 1993.

[13] L.J. Cimini, "Analysis and simulation of a digital mobile channel using orthogonal frequency division multiplexing," *IEEE Trans. on Commun.*, vol. 33, no. 7, pp. 665–675, July 1985.

[14] P.J.W. Melsa, R.C. Younce, C.E. Rohrs, "Impulse response shortening for discrete multitone transceivers," *IEEE Trans. on Commun.*, vol. 44, no. 12, pp. 1662–1672, Dec. 1996.

[15] M. G. Bellanger, G. Bonnerot, and M. Codreuse, "Digital Filtering by Polyphase Network: Application to Sample-Rate Alteration and Filter Banks," IEEE Trans. Acoustics, Speech, and Signal Processing, vol. ASSP-24, pp. 109-114, Apr. 1976.

[16] K. Pahlavan and A.H. Levesque, *Wireless Information Networks.* New York, J. Wiley & Sons, 1995.

[17] H. Meyr, M. Moeneclaey, and S. Fechtel, *Digital Communication Receivers: Synchronization, Channel Estimation and Signal Processing.* New York, Wiley, 1998.

[18] W.C. Lindsey, C.M. Chie, "A survey of digital phase-locked loops," *Proceedings of the IEEE*, vol. 69, no. 4, pp. 410–431, Apr. 1981.

[19] P. Robertson, S. Kaiser, "Analysis of the effect of phase-noise in orthogonal frequency division multiplex (OFDM) systems," in Proc. *ICC '95*, pp. 1652–1657, Seattle, June 1995.

[20] R. Hasholzner, C. Drewes, J.S. Hammerschmidt, "The effects of phase noise on 26 Mb/s OFDMA broadband radio in the local loop systems," in Proc. ACTS Mobile Communications Summit '97, pp. 105–112 Alborg, Denmark, Oct. 1997.

[21] A. Papoulis, *Probability, Random Variables and Stochastic Processes*. 3rd ed., Mc Graw Hill, New York, 1991.

[22] L. Tomba, C. Cangemi, "A semi-analytic tool for the design of OFDM transceivers," in Proc. *IEEE VTC* '99 Fall, pp. 1197–1201, Amsterdam, Sept. 1999.

[23] A.V. Oppenheim, R.W. Schafer, *Discrete-Time Signal Processing.* Prentice Hall, Inc., Englewood Cliffs, NJ, 1989.

[24] L. Tomba, "On the effect of Wiener phase noise in OFDM systems," *IEEE Trans. on Communications*, vol. 46, no. 5, pp. 580–583, May 1998.

	DMT		*FMT*		*FMT-FS*	
	no phn	phn	no phn	phn	no phn	phn
$\mathcal{K} = 64$	0.0	1.0	1.5	2.3	1.5	2.3
$\mathcal{K} = 128$	0.0	1.8	1.6	3.1	1.8	3.2
$\mathcal{K} = 256$	0.0	3.2	2.6	5.2	2.9	5.4

Table 1: Normalized degradation $\mathcal{D}_m$, in dB, for the central subchannel ($m = \mathcal{M}/2$), due to noise and distortion in the absence (no phn) and in the presence (phn) of phase noise ($a_\vartheta = 7.5$). The channel is AWGN with a SNR of 25 dB. Moreover, $\mathcal{M} = \mathcal{K}$ for DMT and FMT, whereas $\mathcal{M} = \lfloor \frac{15}{16} \mathcal{K} \rfloor$ for FMT-FS.

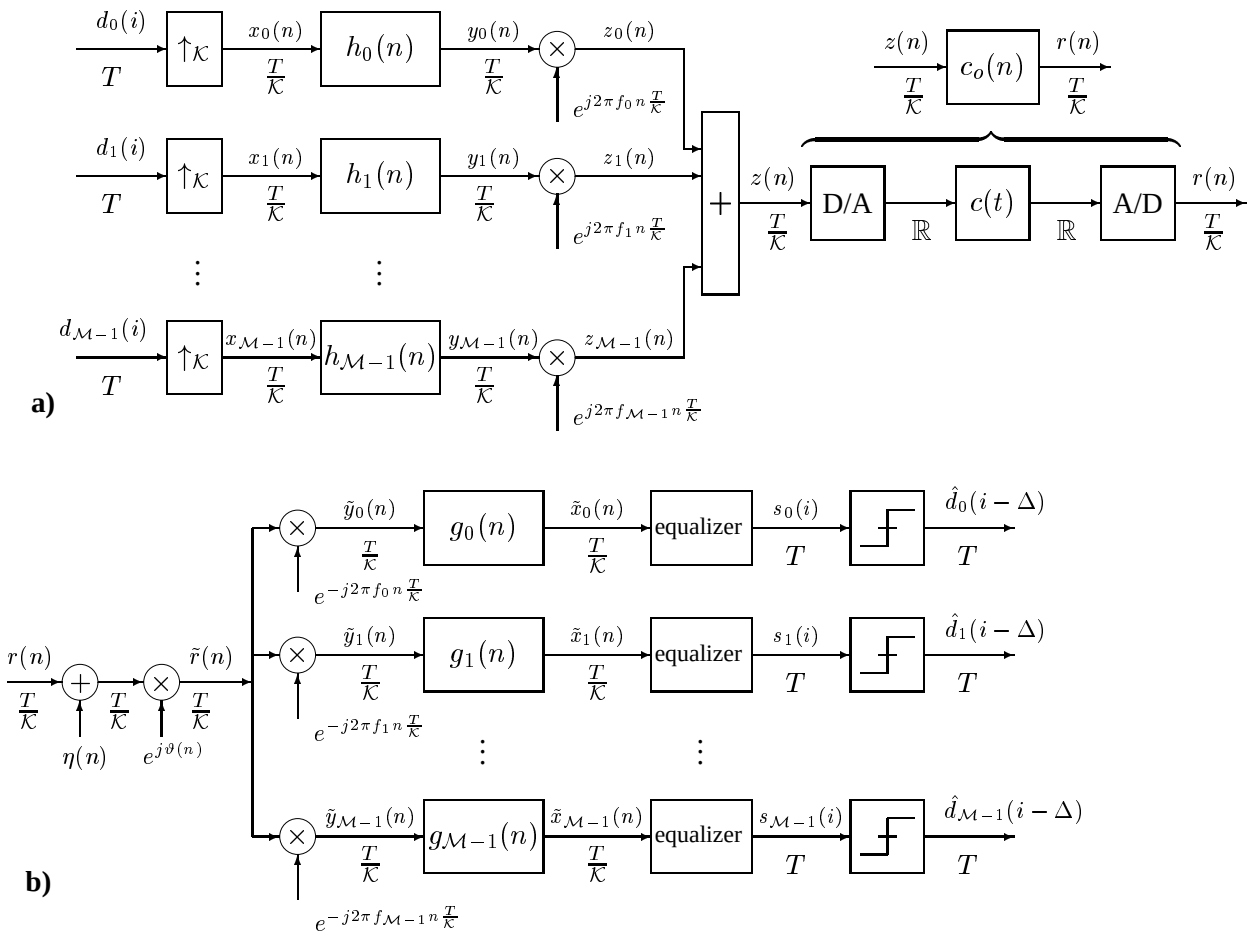

Figure 1: Baseband block diagram of a filter-bank modulation system: (a) transmitter and radio channel, (b) receiver.

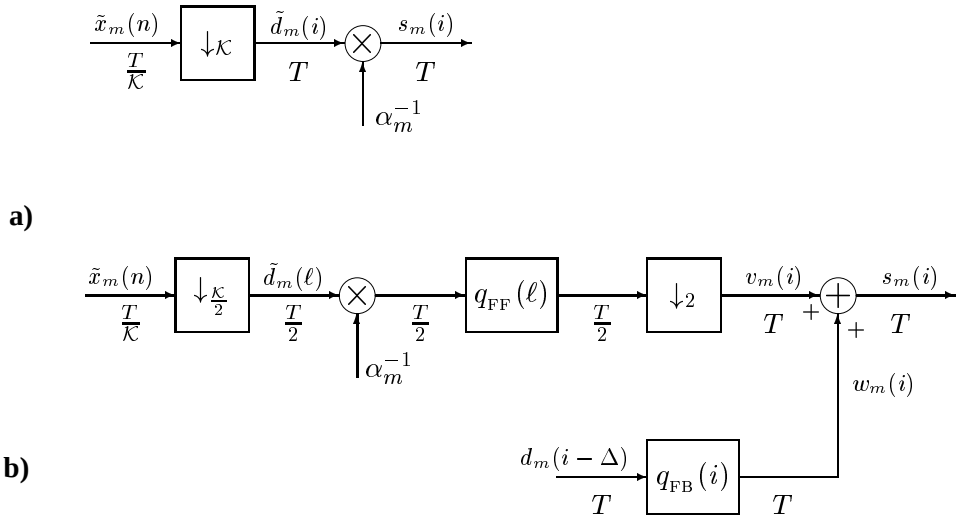

Figure 2: Equalizer structure for the m-th subchannel: (a) DMT, (b) FMT-FS.

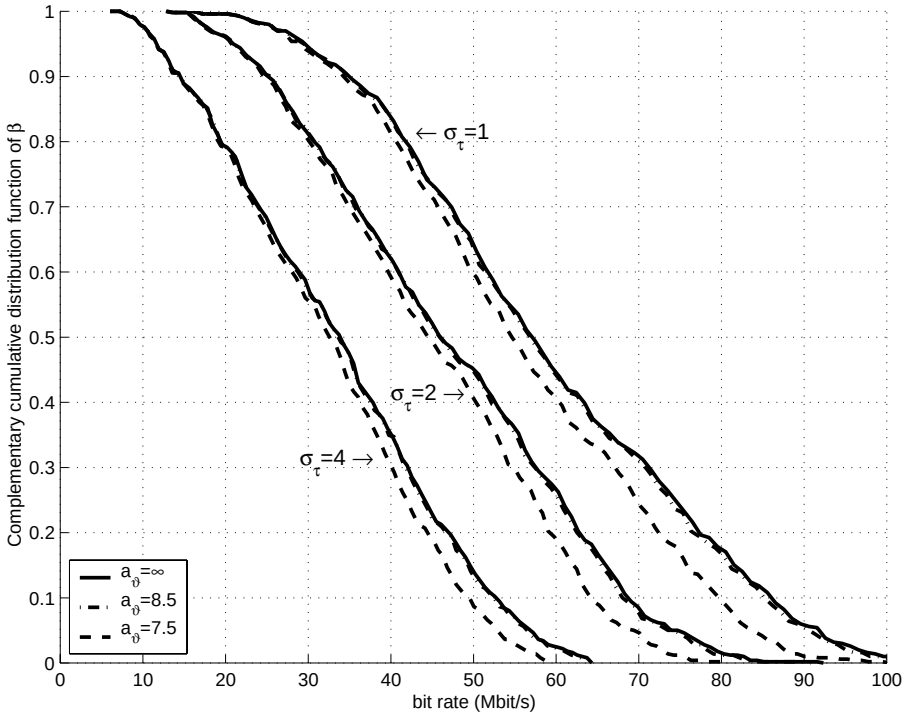

Figure 3: Achievable bit rate for DMT for various choices of a_ϑ and σ_τ. $\mathcal{K} = \mathcal{M} = 64$, $\mathcal{V} = 4$, $f'_\vartheta = 1$ kHz, $f''_\vartheta = 10$ kHz, $b_\vartheta = 4$, $c_\vartheta = 10.5$, SNR$= 25$ dB.

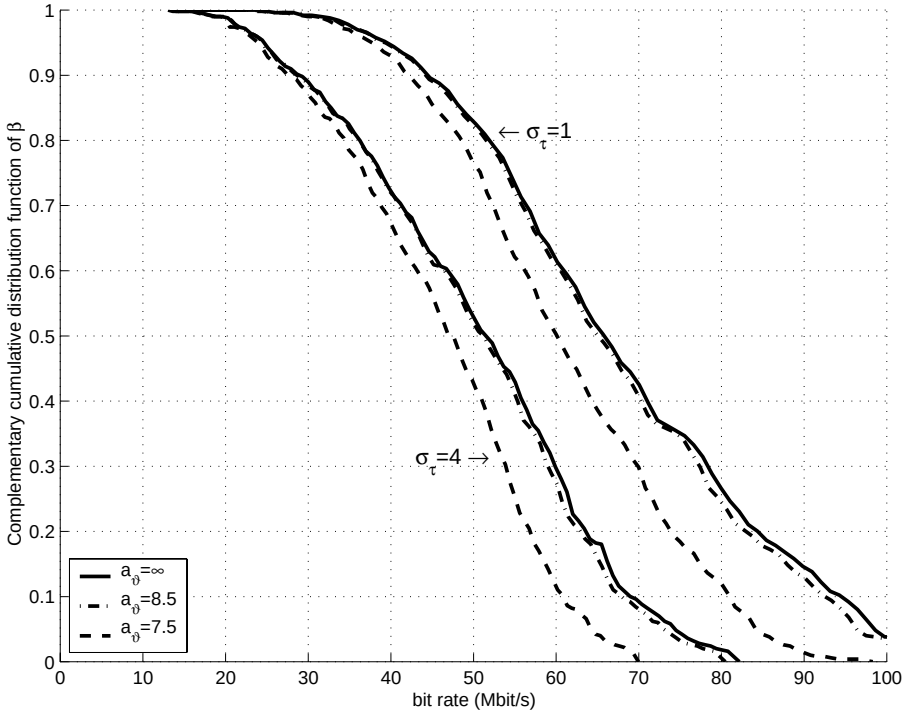

Figure 4: Achievable bit rate for DMT for various choices of a_ϑ and σ_τ. $\mathcal{K} = \mathcal{M} = 128$, $\mathcal{V} = 8$, $f'_\vartheta = 1$ kHz, $f''_\vartheta = 10$ kHz, $b_\vartheta = 4$, $c_\vartheta = 10.5$, SNR$= 25$ dB.

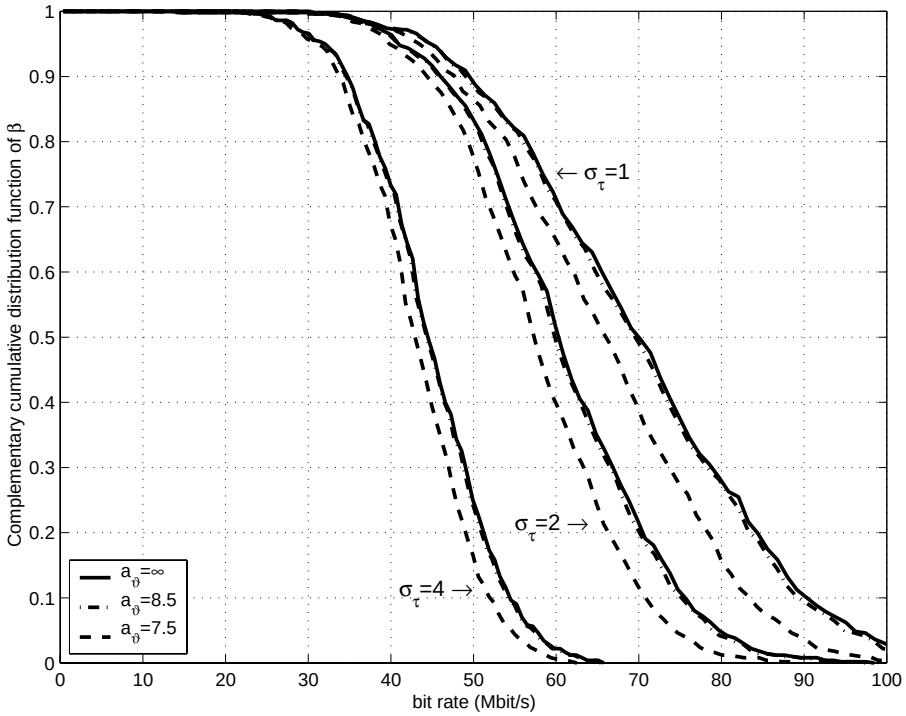

Figure 5: Achievable bit rate for FMT for various choices of a_ϑ and σ_τ. $\mathcal{K} = \mathcal{M} = 64$, $\mathcal{V} = 2$, $f'_\vartheta = 1$ kHz, $f''_\vartheta = 10$ kHz, $b_\vartheta = 4$, $c_\vartheta = 10.5$, SNR$= 25$ dB.

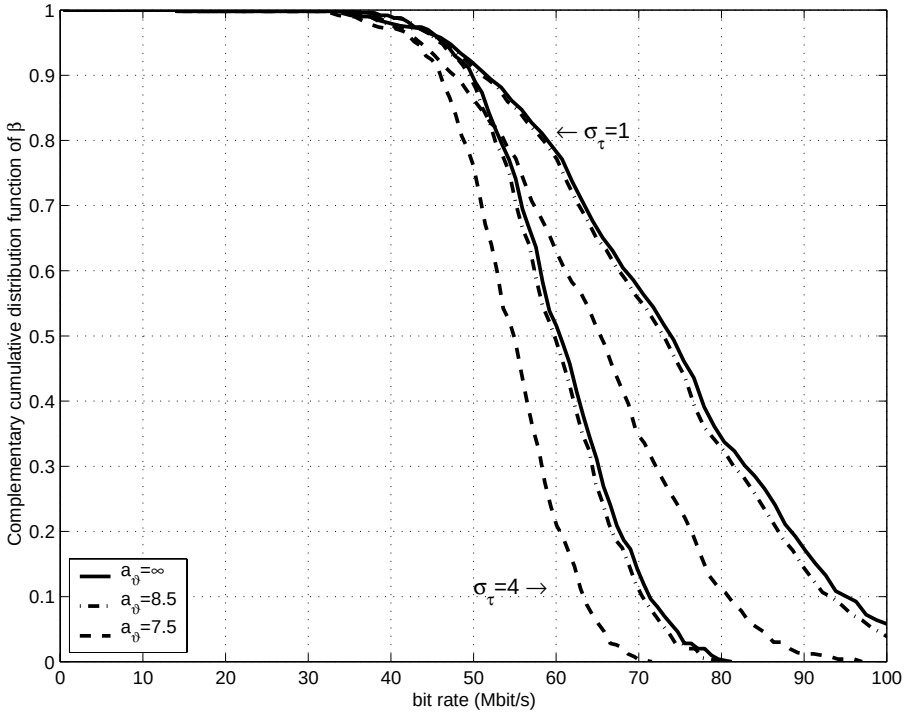

Figure 6: Achievable bit rate for FMT for various choices of a_ϑ and σ_τ. $\mathcal{K} = \mathcal{M} = 128$, $\mathcal{V} = 2$, $f'_\vartheta = 1$ kHz, $f''_\vartheta = 10$ kHz, $b_\vartheta = 4$, $c_\vartheta = 10.5$, SNR$= 25$ dB.

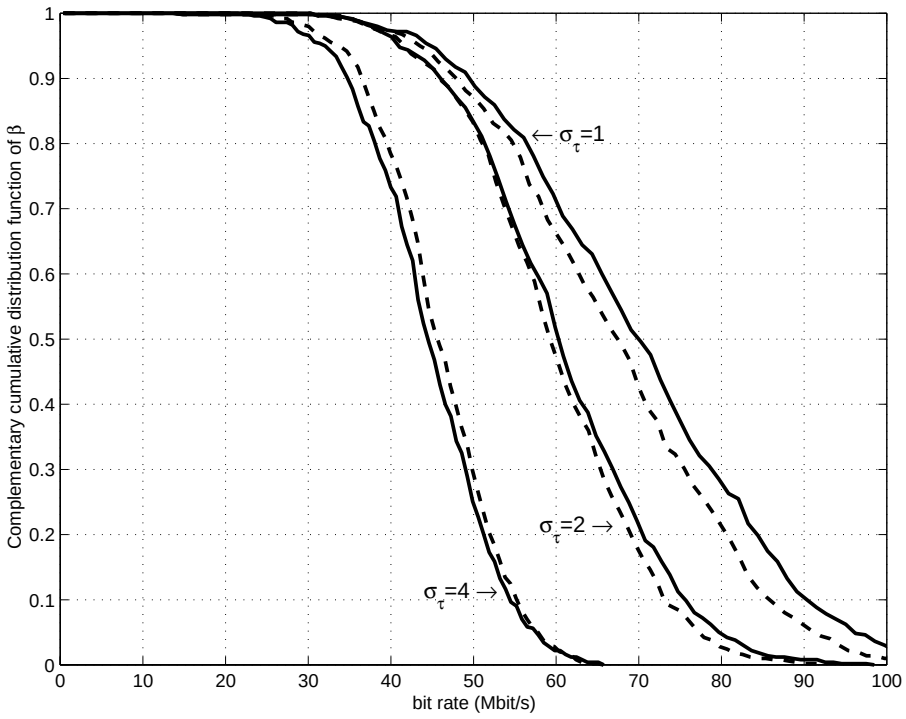

Figure 7: Comparison, in terms of achievable bit rate, between FMT and FMT-FS. Solid lines: FMT with $\mathcal{K} = \mathcal{M} = 64$, DFE(16,15); dashed lines: FMT-FS with $\mathcal{K} = 64$, $\mathcal{M} = 60$, DFE(16,8).

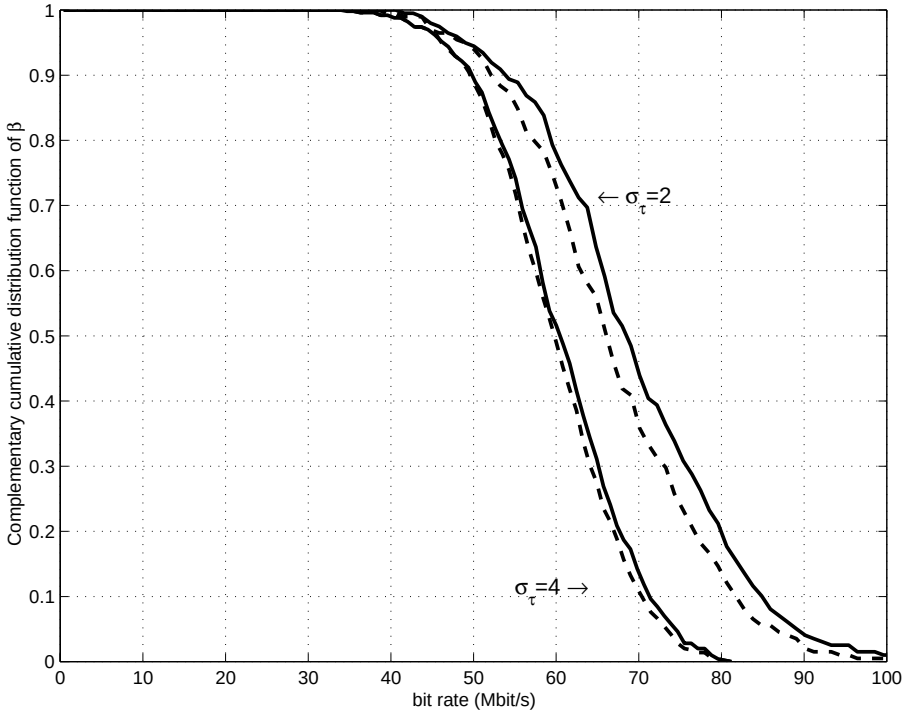

Figure 8: Comparison, in terms of achievable bit rate, between FMT and FMT-FS. Solid lines: FMT with $\mathcal{K} = \mathcal{M} = 128$, DFE(16,15); dashed lines: FMT-FS with $\mathcal{K} = 128$, $\mathcal{M} = 120$, DFE(16,8).